From Mechanical Machining Technology: A New Solution that Integrates Blades to the Implant to Control the Stress to the Peri-Implant Cortical Bone

Mauro Ferri , Marco Guzzo , Hiroyuki Omori , Yuma Hazama , Nicodemo Vittorio Masotta , Botticelli Daniele *

Posted Date: 23 September 2024

doi: 10.20944/preprints202409.1751.v1

Keywords: bone loss; cortical decompression; peri-implant resorption; osseointegration with autologous bone; alveolar precision

Article

From Mechanical Machining Technology: A New Solution that Integrates Blades to the Implant to Control the Stress to the Peri-Implant Cortical Bone

Mauro Ferri [1], Marco Guzzo [2], Hiroyuki Omori [3], Yuma Hazama [3], Nicodemo Vittorio Masotta [4] and Daniele Botticelli [5,*]

[1] Private Practice, 130001 Cartagena de Indias, Colombia. medicina2000ctg@hotmail.com
[2] Senior Mechanical Industrial Engineer @ Brenta Engineering / Leader Medica S.r.l.; marco.guzzo@brentaengineering.it
[3] Department of Oral Implantology, School of Dentistry, Osaka Dental University, 8-1 Kuzuhahanazonocho, Hirakata, Osaka, Japan. (H.O.) last_samurai_1206@me.com; (Y.H.) y.hazama.d@gmail.com
[4] Private practice, 88074-Crotone, Italy. nicodemo.masotta@gmail.com
[5] ARDEC Academy, 47923 Rimini, Italy
* Correspondence: daniele.botticelli@gmail.com

Abstract: Background: To prevent excessive compression of the cortical layer, which can lead to marginal bone loss, various companies have introduced specialized drills. However, these drills often lack the necessary precision, as the operator's hand may not be stable enough to prevent ovalization and over-widening, nor precise enough to maintain coaxial alignment. Therefore, the aim of this study was to develop a device capable of achieving calibrated cortical preparation in terms of both dimension and coaxiality. Methods: A machining technology based on drilling principles was employed to create the device. Results: Nine blades were incorporated between the transmucosal neck and the implant threads, enabling the blades to cut the cortical bone coaxially during the implant insertion process. Conclusions: The implant with integrated blades was engineered to facilitate precise cortical bone preparation, ensuring both accurate dimensions and coaxial alignment. This ensures that the radial compressive stresses transmitted from the implant to the peri-implant bone during surgery can be precisely controlled. The experimental study outcomes discussed in this article validate the effectiveness of the implant design.

Keywords: bone loss; cortical decompression; peri-implant resorption; osseointegration with autologous bone; alveolar precision

1. Introduction

One of the preliminary operations that must be performed for the installation of a dental implant in the alveolar bone is to properly prepare for osteotomy of the recipient sites using special tools. The most common osteotomy preparation system uses drill bits. However, ultrasonic [1–7] or sonic [8–11] devices have also been successfully applied.

The customized, large-scale production of cutting-edge implants represents a significant application within the dental field, including the additive manufacturing [12]. Implants have also been designed to compact bone debris around them, aiming to promote better healing and osseointegration [13]. Also implants that increase such as Through the technology of chip removal, the procedure creates an osteotomy of calibrated dimensions in depth and diameter. While the depth of the osteotomy preparation is adjusted to the length of the implant, the diameter is based not only on that of the implant but also on the quality of the alveolar bone, which may have different hardnesses [1,15–17]. Most implants on the market have threads, and osteotomy is generally prepared

 doi:10.20944/preprints202409.1751.v

with a smaller diameter than that of the implant including threads [18–24]. To achieve the best stability of the implant and avoid damaging compression of the alveolar bone, the clinician calibrates the diameter of the osteotomy to the hardness of the bone; that is, the harder the bone, the larger the diameter. Nevertheless, a compression on the bone, especially in the presence of a hard cortical layer, might result in marginal bone resorption [25–31]. To prevent such issues, various implant systems have introduced specialized drills designed to expand the cortical area of the osteotomy. However, performing this step manually doesn't ensure the required accuracy, as the operator's hand may lack the necessary steadiness to prevent ovalization or excessive widening, and may not maintain perfect coaxial alignment.

Moreover, during installation, the implant often follows the path of least resistance through the bone, potentially deviating from the intended trajectory, even if the operator tries to adjust during the threading process. Hence, the aim of the present study was to obtain a calibrated cortical preparation in terms of dimensions and coaxiality.

2. Founding Paradigms

For this purpose, blades were made between the thread and transcortical collar of the implants.

Such blades can widen the cortical layer during implant insertion at a calibrated diameter and depth with perfect coaxiality with the implant (Figure 1).

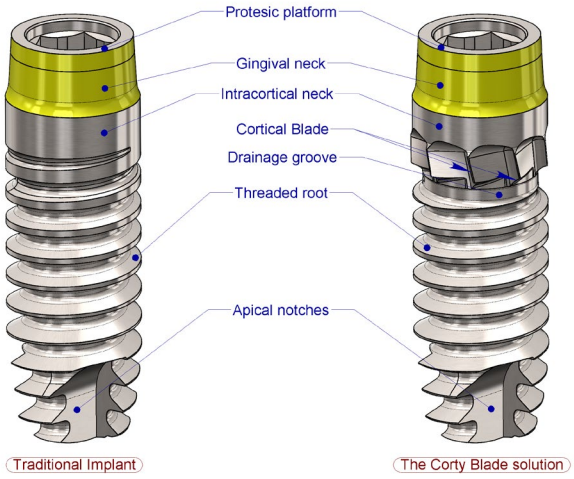

Figure 1. Comparison between a traditional solution and the innovative implant configuration.

Because the blades widen a pre-existing cylindrical hole, the typical operating principle to be adopted to provide them with the desired function is based on machining technology by drilling.

With more than one implant revolution to perform the drilling, it is necessary to use more than one blade; otherwise, the depth for each revolution would be excessively high, resulting in the formation of big chips and a possible stuck of the implant as soon as the blade penetrates the cortical layer.

For these blades to function properly and to attack the cortical bone in the axial direction of the screwing, a special drainage groove must be created between the end of the coronal thread and the cortical blades in order to create the necessary spaces for the cutting edges of the latter (Figure 2).

 doi:10.20944/preprints202409.1751.v

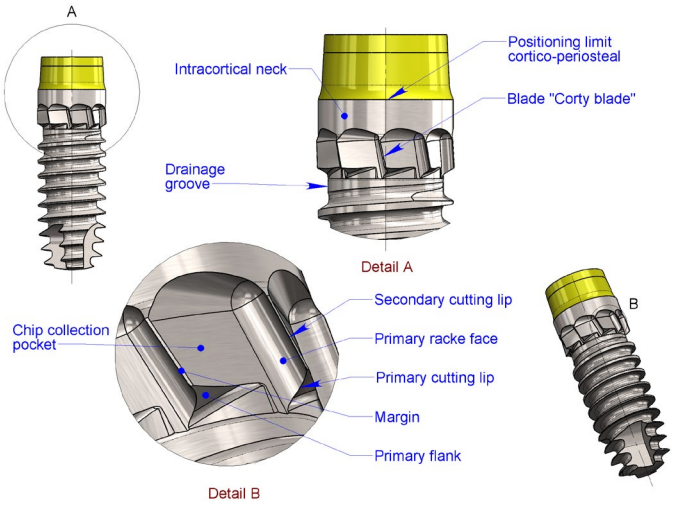

Figure 2. Detail of blades and drainage groove - parts nomenclature.

The blades can have different working diameters. The difference between the diameter of the hole machined by the blades and that of the trans-cortical collar can be simply called the blade differential or Blade Diameter Differential (BDD).

The BDD can be neutral if it corresponds to the diameter of the trans-cortical cylinder, without causing any compressive/decompressive effect; positive when a circumferential marginal space is created between the cortical bone and the trans-cortical cylinder, with a decompressive effect; and negative when the maximum diameter of the blade is smaller than that of the trans-cortical cylinder, so that a certain, but controlled, interference with the cortical bone layer is obtained, with a compressive effect (Figure 3).

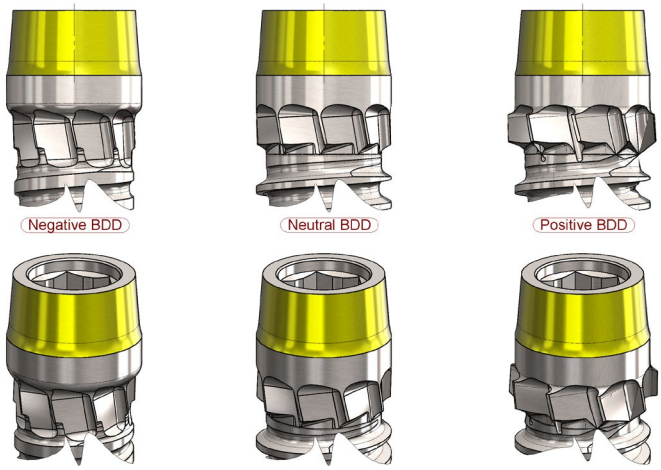

Figure 3. Schematic representation of BDD differential types.

In any case, controlled decompression/compression would be targeted only at the area of the trans-cortical cylindrical portion by means of a mechanical removal process performed by the blades after the complete insertion of the implant thread into the cortical bone.

Therefore, the compression generated by the thread in the intermediate stages of screwing would remain. However, because of the subsequent action of the blades and the relief groove created underneath them, this would be a transient compression, as it would only be applied for a short

 doi:10.20944/preprints202409.1751.v

period of time required for the thread ridges to pass into the cortical bone, which only ends their course in the medullary bone.

The flutes (grooves) used to create the cutting edges of the blades generate the conditions for the bone chips produced to be, in the initial phase, partly expelled into the immediate peri-implant vicinity, and then, as the blades penetrate the cortical bone, forced into the prepared osteotomy. Once this is filled, before the transcortical collar acts as a plug, the flutes expel the chips in excess towards the external surface, eventually promoting bone regeneration (Figures 4–6).

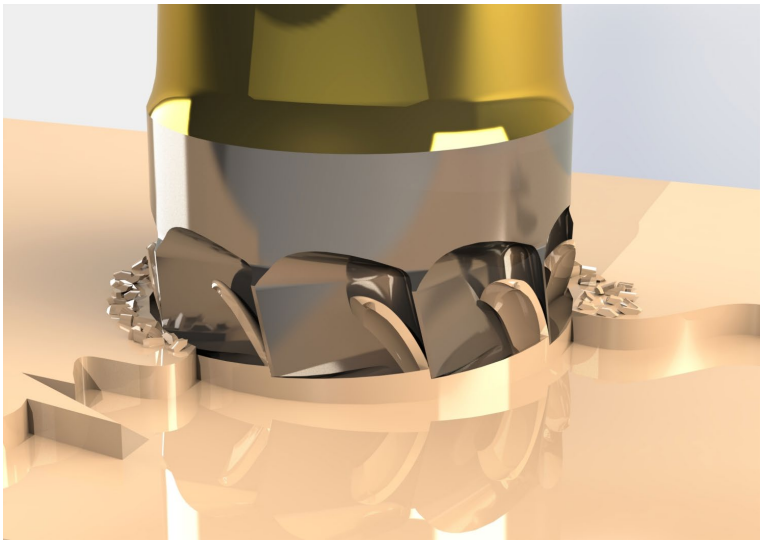

Figure 4. Conceptualization of the blade effect at end of implant placement.

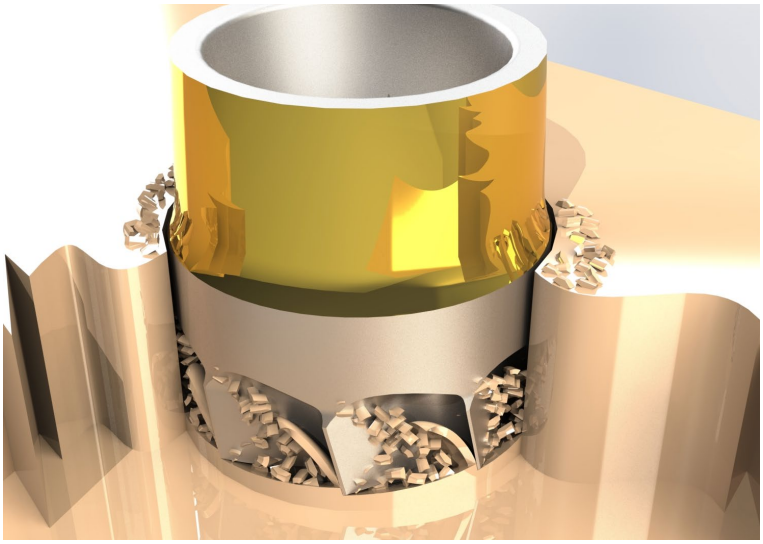

Figure 5. Conceptualization of the blades effect at the end of implant placement.

 doi:10.20944/preprints202409.1751.v

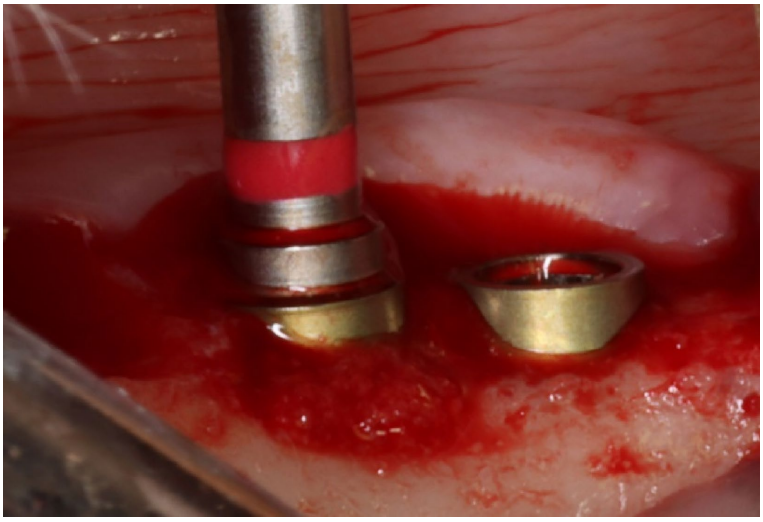

Figure 6. Expulsion of excess autologous material from blade cavities, in vivo (dog).

2.1. Description of the Implant®®

The reference dimensions and their nomenclature are shown in **Error! Reference source not found.**. The implant chosen as an example (CortyBlade®® Leader Medica s.r.l. via Giacinto Longhin 11, Padova, PD, Italy) is determined by a nominal length (Hn) of 10 mm, a nominal external thread diameter of 3.75 mm (d1), a transmucosal neck height (Hctm) of 1.8 mm, a transcortical collar diameter (d4) of 3.75 mm, an external blade diameter (d5) of 3.85 mm and a prosthetic platform diameter (d6) of 3.4 mm.

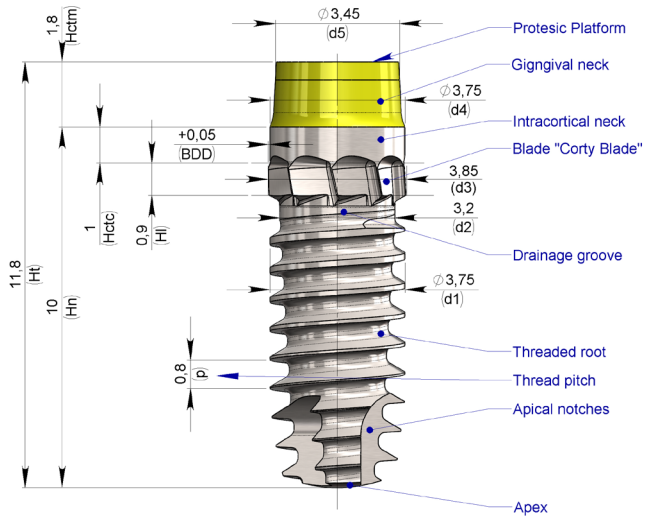

Figure 7. Plant reference dimension nomenclature.

2.2. Mechanics of Bone Chip Formation

Bone chips are produced, during the screwing of the implant, by the primary cutting edge at the lower end of the 'wedge-shaped' blades, which forms the implant, i.e., the main part for producing the osteotomy (**Error! Reference source not found.**a).

The 'wedge' of the primary cutting edge of the blades, rotating in solidarity with the tool, insinuates itself by indentation into the material to be machined. This is due to the action of the cutting edge from which arises an inclined surface, with respect to the working direction, known as the tool's rake upper face. The insinuation of the cutting-edge causes, by plastic deformation or fracture, the separation of a sheet and the subsequent sliding over each other of contiguous layers of material. These, while retaining a certain residual ductility, stack up to form a sort of interconnected

 doi:10.20944/preprints202409.1751.v

and continuous multilayer sandwich, which, as they slide across the upper rake face of the tool, form chips. This principle of action could be well approximated by Merchant's model [3] for isotropic materials (Figure 8).

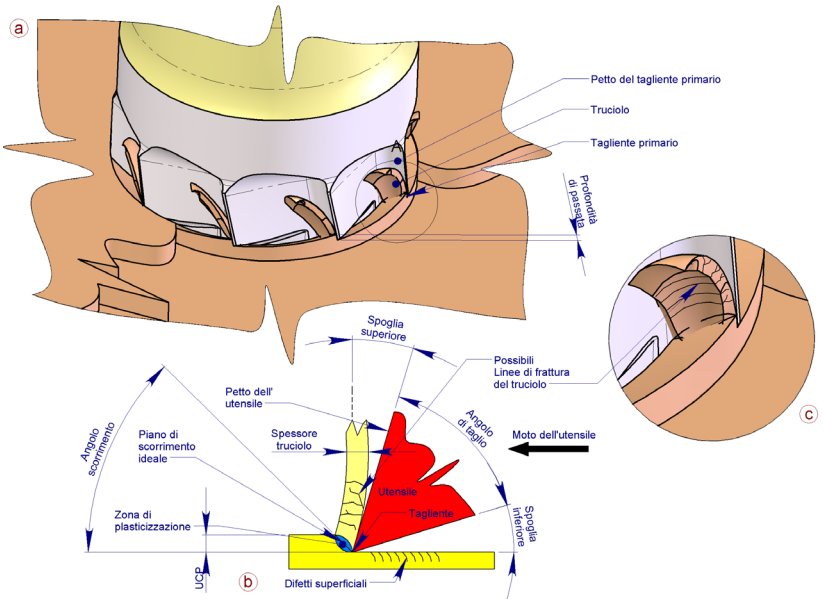

Figure 8. Graphical model of chip formation mechanism.

It must now be considered that cortical bone, for which processing the blades are specifically intended, is a markedly anisotropic material consisting of hierarchical structures [32] and different resistances to processing depending on whether this occurs along the transverse, parallel, or normal directions of the osteons [33–35].

It follows that Merchant's model [36] limits the correct representation of the mechanism of chip formation in cortical bone, as it assumes that the material is perfectly isotropic.

Nomura et al. [37] determined that the direction of the osteons in the human mandible follows the direction of the main axis typical of 'horseshoe' bone. Transposing these results to the situation of a dental implant (Figure 9) to the processing carried out by the implant, it can be seen that the direction in which the blades face the osteons is always different (Figure 9). This is also due to the circular motion in which they move. An identical observation was made by Zhang et al. [36] on the advanced machining of hard tissue studies.

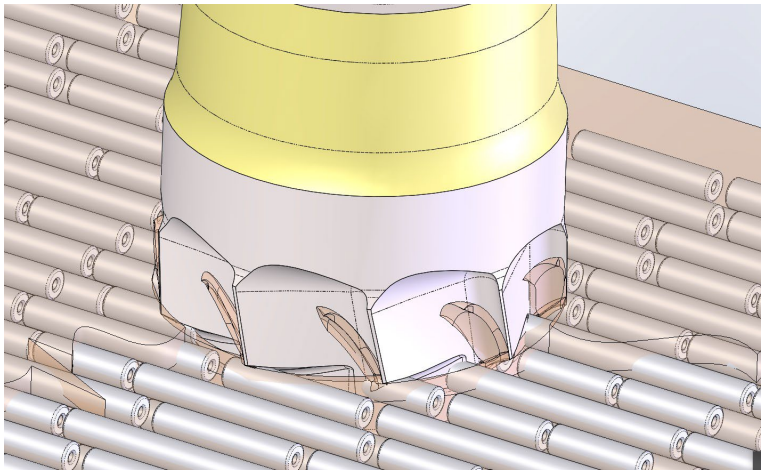

Figure 9. Conceptualization of the distribution and orientation of osteons with respect to the placement of the implant.

However, the cutting procedures are generally performed in multiple directions, so Merchant's model [36] can still provide a good reference for the design of tools planned for bone use [34].

 doi:10.20944/preprints202409.1751.v

Thus, bone chips produced by machining can present different structural conformations. Liao et al. [39] identified three mechanisms of chip formation: - shear cutting; - mixed shear/fracture cutting; - fracture cutting. Not surprisingly, the conformation of the bone chip is mostly independent of the direction of shear with respect to the orientation of the osteons but is more influenced by the depth of the pass.

Liao et al. [39] showed that regardless of the orientation of the osteons, i) an Uncut Chip Thikness (UCP) between 0 and 20 μm produces a continuous, flowing chip (produced by shear cutting mechanism) in bovine cortical bone, which can also curl up; ii) between 20 and 80 μm it produces a continuous, segmented chip (mixed shear/fracture cutting mechanism); iii) between 80 and 150 μm there is a formation of discontinuous chips (fracture cutting mechanism), which also fracture coarsely. However, non-viable cortical bone samples taken from bone femurs were used, which were deprived of the hydration provided in vivo by the bone-feeding fluids normally provided by the Haversian system.

On the other hand, Linares et al. [40] investigated cutting conditions using fresh non-viable bovine bone, artificially feeding the Haversian system of the cortical layer with saline solution, thus coming much closer to reproducing natural hydration of the tissue. Under these conditions, with the same UCT, similar conclusions as Liao et al. [39] were drawn in terms of type of chip formed. However, the hydrating effect of the fluid in the cutting zone formed a chip parallel to the cutting surface (tool chest) instead of curling forward. It was further shown an optimal finishing of the surfaces machined in the presence of fluid in the Haversian canals, leaving the canals and canaliculi open, that is, without obstructing them due to crushing or tearing of the material [40].

2.3. Defining the Type of Swarf to be Produced by the Blades

For the application presented in the present this study, a continuous and flowing chip, possibly curling up, should be avoided because it can clog the blade collection grooves by tangling [41], forming a large body, generating strong friction against the walls of the implant osteotomy, and exerting a non-negligible pressure on the newly worked bone, potentially damaging it.

A coarse discontinuous chip obtained mainly by fracture can produce the same problems as flowing chips. In addition, the fact that it was obtained by fracture could trigger microcracks in the freshly machined surface, which could promote the propagation of deeper fractures in the bone in the immediate future. Furthermore, formation by fracture is synonymous with surface roughness [39], and thus causes significantly more damage to the area where the cut was made.

On the other hand, a segmented continuous chip could be ideal for the application in the present study. First, because the surface finish is not too rough [39], it affects only small, shallow portions of bone. Second, because it is equipped with predetermined, small-sized segmentation lines, it could easily brittle into infinitesimal chips, which are much more suitable to fill the cavity of the blades without causing further damage to the newly machined bone walls, because they are more easily adaptable to the shape of the collection spaces around the blades. Therefore, a continuous, segmented chip type should be adopted as the basis of the blade operation.

3. The Solution®® in Practice

3.1. Parameters at the Main Cutting Edge

3.1.1. Definition of Blade Vertex Angle

The angle at the vertex of the blades is denoted as β (**Error! Reference source not found.**). This angle, as with a drill bit, influences numerous machining parameters such as:

1. **Axial penetration thrust:** The smaller the angle, the lower the thrust required for the blade to penetrate the bone [34].
2. **Self-alignment capability:** The greater the angle, the lower is the alignment capability [42].
3. **Chip width:** The smaller the angle, the larger the normal cross-section of the chip produced [42].
4. **Chip thickness**: The smaller the angle, the smaller is the UCT thickness of the chip.

 doi:10.20944/preprints202409.1751.v

5. **The quantity of heat generated is as follows:** the wider the angle, the greater the creep deformation of the materials, and thus, the greater the heat produced [42].

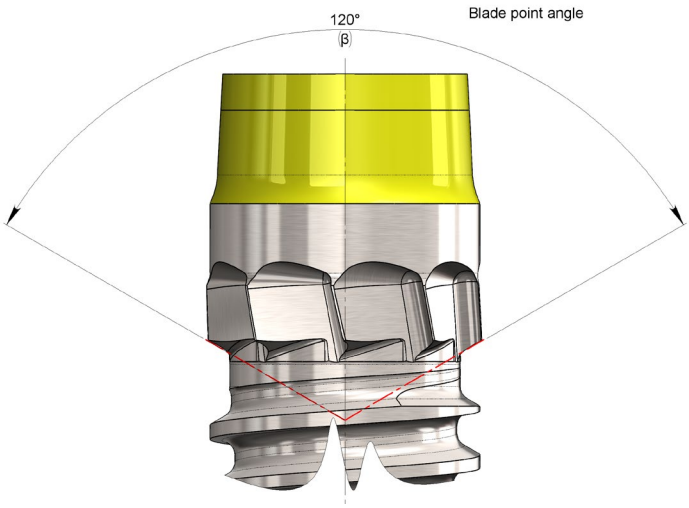

Figure 10. Representation of the apex angle.

The most desirable characteristic of blades is to maintain a good degree of self-alignment with the screw direction of the implant, preventing external forces, such as the thrust exerted by the operator, to deviate from the desired direction. To this end, a vertex angle β tending towards 90° has been suggested [43].

At the same time, however, there is a need to keep the screwing torque of the implant as low as possible to facilitate insertion by the operator working in confined spaces. In fact, the lower the applied external stress, the better is the desired trajectory maintained.

Considering the limited extension of the main cutting edge of the blades, compared with a hypothetical conventional drill bit operating with the same diameter, the penetration thrust can be considered negligible. However, the resistance torque acting near the outer diameter of the blades remained relatively high. To limit the drilling torque, the use of a vertex angle β between 110° and 140° has been suggested [42].

The increased heat produced by using any tip angle can be considered negligible in this case, as the rotation speed of the blades is very limited because the system is expected to be tightened either with a contra-angle handpiece, setting it at a low rotation speed (≤ 20 rpm), or manually with a ratchet.

Considering the standardized dimensions of the tools available on the market for blade manufacturing, a β vertex angle of 120° was chosen. This decision was made because it was considered that penetration forces are generated with sufficient intensity by the thread of the implant (even in a low-density pith), while the torque required for the blades' action is low while maintaining a non-negligible self-aligning action.

3.1.2. Definition of the Upper Rake Angle of the Main Cutting Edge, α

Conventionally, for a drill, the variables and cutting parameters are assumed to be localized at the outermost diameter of the drill, as they may vary depending on the position chosen for their characterization because of the typical morphology of the tool.

The main cutting edge of the blades, derived from that of a traditional drill bit, has an upper face of the tool that forms an angle δ with respect to the cutting direction. With respect to the plane normal to the same cutting direction, the tool's upper face forms an angle α, known as the top rake angle, which can be zero if it is perpendicular to the cutting direction vector (δ = 90°), positive if it forms an obtuse angle (**δ>** 90°), and negative if it forms an acute angle (**δ** < 90°) respect to the cutting direction (**Error! Reference source not found.**).

Preprints.org (www.preprints.org) | NOT PEER-REVIEWED | Posted: 23 September 2024 doi:10.20944/preprints202409.1751.v

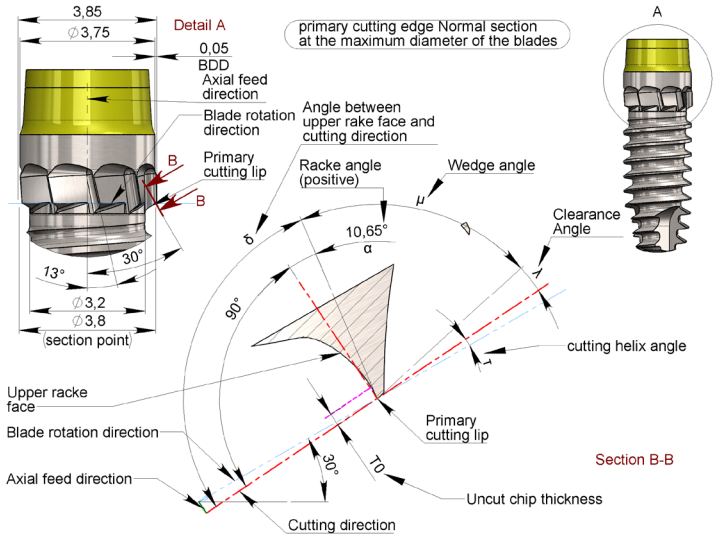

Figure 11. Normal section to the primary cutting edge at the maximum blade diameter.

The rototranslation of the implant during the screwing phase produces a penetration movement of the blades according to a precise inclination, called the working direction, corresponding to the helix angle of the implant thread.

The helix angle ψ, conventionally adopted for the external thread diameter d_1, is determined by

$$\psi = \operatorname{atan}\left(\frac{p}{\pi * d_1}\right) = \operatorname{atan}\left(\frac{0.8\ mm}{\pi * 3.8\ mm}\right) = 3.834° \quad (1)$$

However, the action diameter of blade d_3 does not necessarily coincide with the external diameter of thread d_1 because it depends on the Blade Differential Diameter (BDD) interference/play to be impressed according to the desired biodynamic requirements for the cortical bone.

If, for example, a differential is to be imposed on the blades BDD = +0.05 mm at a thread diameter d_1 = 3.75 mm, the diameter of the blades d_3 can be determined by the following formula:

$$d_3 = d_1 + 2 \times (BDD) = 3.75\ mm + 2 \times (+0.05\ mm) = 3.85\ mm \quad (2)$$

The angle of the working direction ψ_1 adopting $\mathbf{d_3}$ instead of $\mathbf{d_1}$ would become:

$$\psi_1 = \operatorname{atan}\left(\frac{p}{\pi * d_3}\right) = \operatorname{atan}\left(\frac{0.8\ mm}{\pi * 3.85\ mm}\right) = 3.784° \quad (3)$$

Because the blade diameter (d_3) can be varied to best suit the biodynamic requirements of the cortical bone, given the negligible differences between ψ and ψ_1, it is preferable to use d_1, which is a constant of the implant, instead of d_4, which is dependent on the BDD to be conferred.

Kalpakjian [41] stated that if the rake angle α is small, that is, tends to 0, the chip tends to form in a discontinuous fragmented type.

Top rake angles of 8° have been use in some studies [39,40]. However, both provide chip formation as a function of the depth of pass (UCP) and not as a function of the rake angle.

In the blades, unlike conventional drill bits, the main cutting edge does not have a linear but a curved profile, owing to their construction method. Therefore, it is also necessary to consider the effect of blade construction geometry on the effective upper rake angle $\boldsymbol{\alpha}$. Starting from the outer diameter of the blades d_3 towards the core diameter of the screw d_2, the geometric effect involves the transformation of the upper rake angle $\boldsymbol{\alpha}$ from positive (**Error! Reference source not found.**) to negative (**Error! Reference source not found.**).

 doi:10.20944/preprints202409.1751.v

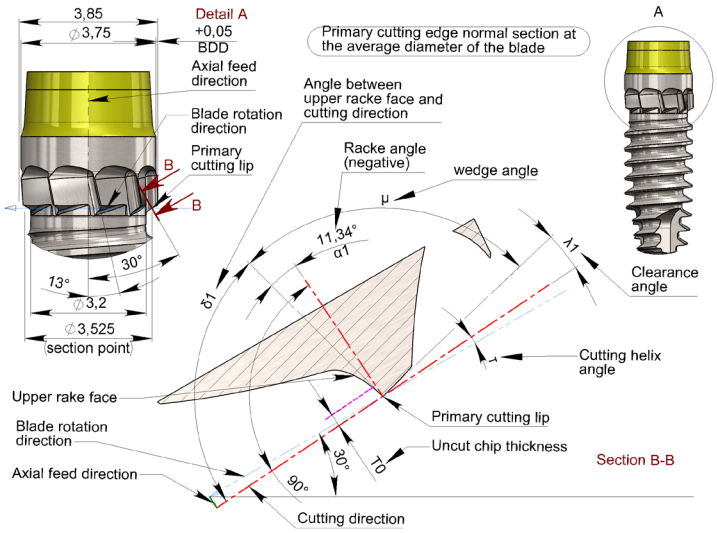

Figure 12. Normal section at the primary cutting edge at the average blade diameter.

To simplify the procedure for determining the upper rake angle α without committing major approximation errors, it is advisable to use the blade helix angle $\boldsymbol{\varepsilon}$ as a reference and then check that the 'real' rake angle α remains within a small geometric variation, arbitrarily set at values close to α = 0° +/- 10° in order to comply with the suggestion from other reports [39–41].

It follows that the helix angle of the blades $\boldsymbol{\varepsilon}$, to obtain a rake angle above the main cutting edge, $\boldsymbol{\alpha}$ = 0°, must be equal to ψ.

It is now necessary to consider that the helix angle $\boldsymbol{\varepsilon}$ of the blades also influences the extraction of the chip from the collecting cavity (and therefore, from the osteotomy). If the helix angle is increased with respect to ψ, the filling of the collecting cavity tends to increase, conveying the chip towards the inside of the osteotomy. If it decreases, it tends to empty, driving the chip outwards. If it coincides with ψ, it tends to leave the swarf at a random filling/ejection depending on the type of swarf that the other operating conditions influence.

For the purpose of the invention, the bone chips should first fill the cavity, as this is supposed to promote the bone regeneration necessary for osseointegration [44–46], and only then achieve their complete filling, as the collecting cavities have a volume smaller than the excavated volume.

The excess bone chip must therefore be evacuated externally, avoiding producing much compression on the walls of the osteotomy, in accordance with the objective of the blades to reduce or control compression on the cortical bone. As a result, it is preferable to give an increased angle differential $\boldsymbol{\varepsilon}$ of +9° (arbitrarily chosen) to give a slightly forced harvesting effect, because the type of continuous segmented chip (brittle), once the cavity is filled, is sufficiently "fluid" to be drained without significantly increasing the compressive effect on the bone.

As mentioned previously, the helix angle of the blades can be determined by

$$\boldsymbol{\varepsilon} = \psi + 9° = \operatorname{atan}\left(\frac{p}{\pi * d_1}\right) + 9° = \operatorname{atan}\left(\frac{0.8\ mm}{\pi * 3.75\ mm}\right) + 9° = 12.834° \qquad (4A)$$

This value can be approximated as an excess without appreciably affecting the desired effect at $\boldsymbol{\varepsilon}$ =13°. The adoption of this angle results in variability (verified at CAD for simplicity) in the rake angle α between

$$\alpha = \begin{bmatrix} +10.65° \\ -11.34° \end{bmatrix}$$

This value falls within the previously established limits to a reasonable degree; therefore, a helix angle **of** $\boldsymbol{\varepsilon}$ = 13° was chosen.

3.1.3. Defining the Clearance Angle below the Main Cutting Edge

The clearance angle of the main cutting edge is denoted as λ, as shown in Figure 13. This allows the secondary flank of the cutting edge to not rub the freshly machined surface while compensating

 doi:10.20944/preprints202409.1751.v

for the even minimal springback that would push it against the tool. It has been suggested that λ should be between 12° and 15° for the cortical bone [47,48]. However, the axial feed pitch per revolution of the implant is very high (0.8 mm/revolution) compared to that of a normal drill (for the diameter in question about 0.05 mm/revolution). The blades are integrated into the dental implant and, therefore, feed with the thread pitch. The helix angle ψ of the latter has already been defined in equation (1) as ψ=3.834°.

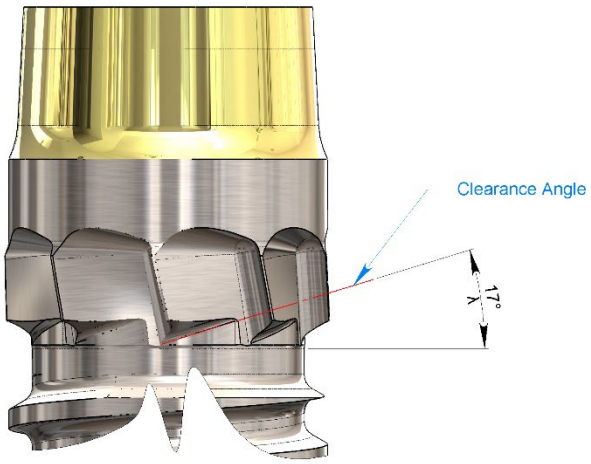

Figure 13. The clearance angle below the main cutting edge.

It is therefore necessary to increase the suggested λ-angle [47,48] (average value 13.5°) by an amount equal to the helix angle ψ of the thread to avoid rubbing of the flank of the main cutting edge on the bone because of the high penetration pitch per revolution, which can be re-determined as:

$$\lambda = \psi + 13.5° = \operatorname{atan}\left(\frac{p}{\pi * d_1}\right) + 13.5° = \operatorname{atan}\left(\frac{0.8\ mm}{\pi * 3.8\ mm}\right) = 17.334° \quad (4B)$$

This could be rounded to unity without incurring excessive approximations, that is λ = 17°.

3.2. Parameters at the Secondary Cutting Edge

The secondary cutting edge (Figure 14) performs the function of scraping, without further incising it, and the transcortical cylindrical surface is machined by the primary cutting edge, cleaning it, detaching any fragments remaining adhered to it, dragging them to the center of the flute of the blades to obtain the filling of the collection cavities, or, once the latter have been filled, guaranteeing their evacuation outside the osteotomy. To perform this function, an upper positive rake angle τ= 40° was arbitrarily chosen.

Preprints.org (www.preprints.org) | NOT PEER-REVIEWED | Posted: 23 September 2024 doi:10.20944/preprints202409.1751.v

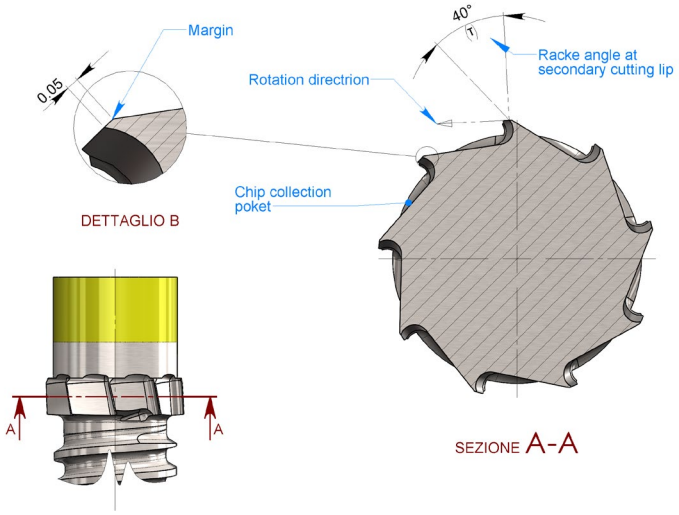

Figure 14. The secondary cutting edge.

To the secondary cutting edge was not assigned a clearance angle. This is because the flank must perform the function of guiding the blades over the intra-cortical cylinder just created by the primary cutting edge. This means that this flank, also referred to as the blade edge, performs the function of restraining external loads that the operator might apply during screwing maneuvers, especially when using a hand ratchet.

The arbitrarily chosen margin geometry of 0.05 mm also helps to keep the friction torque low, which would otherwise increase the screwing torque of the implant, increasing the lateral forces to be applied and, consequently, potentially increasing the axial deflection.

3.3. Defining the Number of Blades

As in the drill bit, the main cutting edges are fed by the pitch p of the thread. Given the number of blades N_b, the axial feed per blade a can be determined from the ratio:

$$a = p/N_b \quad (5)$$

We must now consider that the blades have a vertex angle β, which, as mentioned above, influences the thickness of the chip being machined (UCT). The smaller the vertex angle β, the smaller the chip thickness UCT, according to the following mathematical relationship:

$$UCT = a \times \sin\left(\frac{\beta}{2}\right) \quad (6)$$

Substituting equation (6) for a into equation (5) and solving it for N_b yields the mathematical relationship that links the number of blades to the desired UCT chip thickness, vertex angle β, and thread pitch p:

$$N_b = \frac{p \times \sin\left(\frac{\beta}{2}\right)}{UCT} \quad (7)$$

To obtain the desired chip type (segmented continuous) a depth of cut (UCT) between 20 μm and 80 μm should be used [39]. The adoption of a UCT value at the lower limit, called UCT_0, equal to 20 μm (UCT_0 = 0.02 mm), produces a number of blades N_b equal to

$$N_b = \sin\frac{p \times \cos\left(\frac{\beta}{2}\right)}{UCT_0} = \frac{0.8\ mm \times \sin\left(\frac{120^\circ}{2}\right)}{0.020\ mm} = 34.641 \cong 35 \quad (8)$$

A total of 35 blades were considered excessive because of the delicate construction form that would have to be given to them. In addition, the tools for making them are excessively fragile, and a high number of machining operations would result in high production costs.

The adoption of a depth of cut (UCT) value at the upper limit, called UCT_1 equal to 80 μm (UCT_1 = 0.08 mm), would produce a number of blades corresponding to

$$N_b = \frac{p \times \sin\left(\frac{\beta}{2}\right)}{UCT_1} = \frac{0.8\ mm \times \sin\left(\frac{120^\circ}{2}\right)}{0.080\ mm} = 8.660 \cong 9 \quad (9)$$

 doi:10.20944/preprints202409.1751.v

Nine blades would be acceptable from the perspective of production economy. Furthermore, because the number of blades chosen is a multiple of the number of predetermined apical notches (N_i =3), the latter could be banded with the blades, creating considerable advantages during implant processing.

By adopting N_b =9 blades, the depth of cut actually applied (UCT_{eff}) by a single blade can be re-determined as

$$UCT_{eff} = \frac{p \times sin\left(\frac{\beta}{2}\right)}{N_b} = \frac{0.8\ mm \times sin\left(\frac{120^\circ}{2}\right)}{9} = 0.077\ mm \quad (10)$$

This value is within the set UCT limit for obtaining continuous segmented chips; therefore, a number of blades equal to N_b =9 should be adopted.

4. Discussion

Almost all existing dental implants require a clinical protocol that includes insertion by interference of the threads with both the medullary and cortical bones. This was done to provide the implant with the greatest possible primary stability even in cases of low-density bone.

Due to the conformation of most implants on the market, the highest stability is obtained in the cortical layer through compression of the implant neck and threads towards the bone. However, in the presence of a hard cortical layer, the implant can become stuck into the bone or break it if the crest is thin.

On the other hand, in terms of primary stability, an excessively large osteotomy preparation, insufficient screwing torque, or poorly resistant bone can lead to micromobility of the implant, especially in tapered implants, where tapering acts both as an amplifier of thread-biting capacity and as an accelerator of 'unscrewing' if adequate boundary load conditions are not achieved (respect for deformations in the elastic field of the bone).

It is therefore essential to carefully dose the 'preload' to be given to the dental implant during the screwing phase, in an attempt to avoid excessive stress transfer from the bone-implant interface to the supporting bone and a possible effect on marginal bone loss [25–31].

Bone is a living tissue, and, as such, even in implant surgery, it must be respected by keeping it as vital as possible. One method of pursuing vitality is to avoid overstressing it mechanically. The solution presented in this study could be the key to controlling bone loss resulting from excessive mechanical stress, generally caused by the interference of the threads/neck of traditional dental implants on the cortical bone portion with the aim of generating primary stability [23,49–52].

To evaluate performance and outcomes, recent animal studies have utilized implants with integrated blades, named Cortyblade(R). In one study involving dogs, implants were placed in the edentulous alveolar ridge, and blades of different diameters were incorporated into the coronal portion of the implants to adjust the preparation of the cortical bone crest [53]. The blade-to-collar diameter variations included -175 μm (inducing marginal bone compression), 0 μm, +50 μm, and +200 μm, creating marginal gaps of corresponding sizes. The results showed that the highest bone crest position was observed with implants having a marginal gap of 50 μm. The cortical blades achieved good osseointegration and facilitated the collection of bone particles, especially in the +200 μm group, which were also incorporated into the newly formed bone.

Cortyblade implants featuring blades with diameters varying by 0 μm, +50 μm, and +200 μm relative to the implant collar were tested in rabbit tibiae [54]. The blades enabled precise contouring of the cortical layer, allowing for controlled decompression in the targeted area. This approach resulted in successful osseointegration, including the integration of the blades, while preserving marginal bone and closing marginal gaps ranging from 0 μm to 200 μm.

In addition, as this new configuration of the implant is potentially able to right-size the implant socket, since they are integrated into the implant, they could provide a further means of controlling the state of compression and/or decompression of the cortical layer, resulting from the unpredictable deviations imposed by the path of least resistance offered by the bone that opposes the pre-established implant positioning.

 doi:10.20944/preprints202409.1751.v

Furthermore, by collecting and forcing bone chips into the implant site, they can promote regeneration and osseointegration of the peri-implant tissues [53,54], potentially accelerating healing time and thus implant stabilization.

Blades eliminate radial cortical compression during implant insertion, without interfering with the primary stability of the implant and promoting optimal osseointegration as found in both studies cited [53,54].

With all the limitations of this study, the research establishes the basic principles for the proposed new solutions. These principles may represent a significant step towards optimizing the clinical protocol and predictability in relation to crestal bone loss.

5. Conclusion

The implant with integrated blades was engineered to facilitate precise cortical bone preparation, ensuring both accurate dimensions and coaxial alignment. This ensures that the radial compressive stresses transmitted from the implant to the peri-implant bone during surgery can be precisely controlled. The experimental study outcomes discussed in this article validate the effectiveness of the implant design.

6. Patents

The innovations described in this article, relating to the CortyBlade®® dental implant, are covered by PCT No. PCT/IB2022/061392.

Author Contributions: Conceptualisation, M.F and M.G.; methodology, M.F., M.G., and D.B; validation, M.F., H.O., Y.H, and V.N.M.; formal analysis, M.G.; investigation, M.G.; resources, M.F., M.G. and D.B.; data curation, M.G. and D.B.; writing-original draft preparation, M.G. and D.B.; writing-review and editing, M.F., M.G., H.O., Y.H., N.V.M, and D.B.; visualisation, H.O., Y.H., N.V.M.; supervision, D.B.; project administration, M.G.; funding acquisition, M.F., M.G, and D.B. All authors have read and agreed to the published version of the manuscript.

Funding: This study was funded by ARDEC Academy and Leader Medica s.r.l..

Institutional Review Board Statement: Not applicable.

Informed Consent Statement: Not applicable.

Data Availability Statement: Data are available on reasonable request.

Conflicts of Interest: M.F., H.O., Y.H., V.N.M and D.B. declare no conflit of interest. M.G. declare conflit of interest.

References

1. Arakji H, Osman E, Aboelsaad N, Shokry M. Evaluation of implant site preparation with piezosurgery versus conventional drills in terms of operation time, implant stability and bone density (randomized controlled clinical trial- split mouth design). BMC Oral Health. 2022 Dec 3;22(1):567. doi: 10.1186/s12903-022-02613-4. PMID: 36463145; PMCID: PMC9719637.
2. Mamidi AR, Gottumukkala SNVS, Mantena SR, Penmetsa GS, Ramesh KSV, Pasupuleti MK. Comparison of clinical and radiological outcomes using crestal approach sinus kit and piezoelectric surgery for sinus membrane elevation: A prospective clinical trial. Dent Res J (Isfahan). 2022 Oct 20;19:88. PMID: 36426279; PMCID: PMC9680697.
3. Bassi F, Cicciù M, Di Lenarda R, Galindo Moreno P, Galli F, Herford AS, Jokstad A, Lombardi T, Nevins M, Sennerby L, Schierano G, Testori T, Troiano G, Vercellotti T, Stacchi C. Piezoelectric bone surgery compared with conventional rotary instruments in oral surgery and implantology: Summary and consensus statements of the International Piezoelectric Surgery Academy Consensus Conference 2019. Int J Oral Implantol (Berl). 2020;13(3):235-239. PMID: 32879928.
4. Fujiwara S, Kato S, Bengazi F, Urbizo Velez J, Tumedei M, Kotsu M, Botticelli D. Healing at implants installed in osteotomies prepared either with a piezoelectric device or drills: an experimental study in dogs. Oral Maxillofac Surg. 2021 Mar;25(1):65-73. doi: 10.1007/s10006-020-00895-y. Epub 2020 Aug 15. PMID: 32803459.

5. Stacchi C, Bassi F, Troiano G, Rapani A, Lombardi T, Jokstad A, Sennerby L, Schierano G. Piezoelectric bone surgery for implant site preparation compared with conventional drilling techniques: A systematic review, meta-analysis and trial sequential analysis. Int J Oral Implantol (Berl). 2020;13(2):141-158. PMID: 32424381.
6. Li X, Lin X, Guo J, Wang Y. The Stability and Survival Rate of Dental Implants After Preparation of the Site by Piezosurgery vs Conventional Drilling: A Systematic Review and Meta-Analysis. Int J Oral Maxillofac Implants. 2020 May/Jun;30(3):e51-e56. doi: 10.11607/jomi.5913. PMID: 32406651
7. Bengazi F, Lang NP, Canciani E, Viganò P, Velez JU, Botticelli D. Osseointegration of implants with dendrimers surface characteristics installed conventionally or with Piezosurgery®®. A comparative study in the dog. Clin Oral Implants Res. 2014 Jan;25(1):10-5. doi: 10.1111/clr.12082. Epub 2012 Dec 12. PMID: 23231427.
8. Sakuma S, Piattelli A, Baldi N, Ferri M, Iezzi G, Botticelli D. Bone Healing at Implants Placed in Sites Prepared Either with a Sonic Device or Drills: A Split-Mouth Histomorphometric Randomized Controlled Trial. Int J Oral Maxillofac Implants. 2020 Jan/Feb;35(1):187-195. doi: 10.11607/jomi.7481. PMID: 31923301.
9. Agabiti I, Botticelli D. Two-Stage Ridge Split at Narrow Alveolar Mandibular Bone Ridges. J Oral Maxillofac Surg. 2017 Oct;75(10):2115.e1-2115.e12. doi: 10.1016/j.joms.2017.05.015. Epub 2017 May 24. PMID: 28623685.
10. Cesaretti G, Lang NP, Salata LA, Schweikert MT, Gutierrez Hernandez ME, Botticelli D. Sub-crestal positioning of implants results in higher bony crest resorption: an experimental study in dogs. Clin Oral Implants Res. 2015 Dec;26(12):1355-60. doi: 10.1111/clr.12467. Epub 2014 Aug 14. PMID: 25123414.
11. Viganò P, Botticelli D, Salata LA, Schweikert MT, Urbizo Velez J, Lang NP. Healing at implant sites prepared conventionally or by means of Sonosurgery ®®. An experimental study in dogs. Clin Oral Implants Res. 2015 Apr;26(4):377-382. doi: 10.1111/clr.12348. Epub 2014 Feb 13. PMID: 24524198.
12. Andreucci, C.A.; Fonseca, E.M.M.; Jorge, R.N. 3D Printing as an Efficient Way to Prototype and Develop Dental Implants. Biomedinformatics 2022, 2, 671–679. https://doi.org/10.3390/biomedinformatics2040044
13. Andreucci, C.A.; Fonseca, E.M.M.; Jorge, R.N. Increased Material Density within a New Biomechanism. Math. Comput. Appl. 2022, 27, 90. https://doi.org/10.3390/mca27060090
14. Velikov S, Susin C, Heuberger P, Irastorza-Landa A. A New Site Preparation Protocol That Supports Bone Quality Evaluation and Provides Predictable Implant Insertion Torque. J Clin Med. 2020 Feb 11;9(2):494. doi: 10.3390/jcm9020494. PMID: 32054122; PMCID: PMC7074433.
15. Elias CN, Rocha FA, Nascimento AL, Coelho PG. Influence of implant shape, surface morphology, surgical technique and bone quality on the primary stability of dental implants. J Mech Behav Biomed Mater. 2012 Dec;16:169-80. doi: 10.1016/j.jmbbm.2012.10.010. Epub 2012 Nov 2. PMID: 23182386.
16. Möhlhenrich SC, Heussen N, Modabber A, Bock A, Hölzle F, Wilmes B, Danesh G, Szalma J. Influence of bone density, screw size and surgical procedure on orthodontic mini-implant placement - part B: implant stability. Int J Oral Maxillofac Surg. 2021 Apr;50(4):565-572. doi: 10.1016/j.ijom.2020.07.003. Epub 2020 Jul 24. PMID: 32713778.
17. Pantani F, Botticelli D, Garcia IR Jr, Salata LA, Borges GJ, Lang NP. Influence of lateral pressure to the implant bed on osseointegration: an experimental study in dogs. Clin Oral Implants Res. 2010 Nov;21(11):1264-70. doi: 10.1111/j.1600-0501.2010.01941.x. PMID: 20626423.
18. Kotsu M, Urbizo Velez J, Bengazi F, Tumedei M, Fujiwara S, Kato S, Botticelli D. Healing at implants installed from ~ 70- to < 10-Ncm insertion torques: an experimental study in dogs. Oral Maxillofac Surg. 2021 Mar;25(1):55-64. doi: 10.1007/s10006-020-00890-3. Epub 2020 Jul 29. PMID: 32725574.
19. Al-Tarawneh SK, Thalji G, Cooper LF. Macrogeometric Differentiation of Dental Implant Primary Stability: An In Vitro Study. Int J Oral Maxillofac Implants. 2022 Nov-Dec;37(6):1110-1118. doi: 10.11607/jomi.9656. PMID: 36450016.
20. Benalcázar-Jalkh EB, Nayak VV, Gory C, Marquez-Guzman A, Bergamo ET, Tovar N, Coelho PG, Bonfante EA, Witek L. Impact of implant thread design on insertion torque and osseointegration: a preclinical model. Med Oral Patol Oral Cir Bucal. 2023 Jan 1;28(1):e48-e55. doi: 10.4317/medoral.25576. PMID: 36173722; PMCID: PMC9805329.
21. Yang B, Irastorza-Landa A, Heuberger P, Ploeg HL. Effect of insertion factors on dental implant insertion torque/energy-experimental results. J Mech Behav Biomed Mater. 2020 Dec;112:103995. doi: 10.1016/j.jmbbm.2020.103995. Epub 2020 Aug 1. PMID: 32882675.
22. Almutairi AS, Walid MA, Alkhodary MA. The effect of osseodensification and different thread designs on the dental implant primary stability. F1000Res. 2018 Dec 5;7:1898. doi: 10.12688/f1000research.17292.1. PMID: 31131085; PMCID: PMC6518436.
23. Romanos GE, Kuyunov O, Sacks D, Calvo-Guirado JL, Delgado-Ruiz R. Apical stability of implants with progressive thread design in vitro, based on clinicians with different levels of experience. J Periodontol. 2019 Nov;90(11):1320-1324. doi: 10.1002/JPER.18-0680. Epub 2019 Jul 1. PMID: 31162678.

24. Eom TG, Kim HW, Jeon GR, Yun MJ, Huh JB, Jeong CM. Effects of Different Implant Osteotomy Preparation Sizes on Implant Stability and Bone Response in the Minipig Mandible. Int J Oral Maxillofac Implants. 2016 Sep-Oct;31(5):997-1006. doi: 10.11607/jomi.4165. PMID: 27632253.
25. S. Nimbalkar, P. Dhatrak, C. Gherde e S. Joshi, «A review article on factors affecting bone loss in dental implants,» Materials today: Proceedings, vol. 43, n. 2, pp. 970-976, 2021.
26. Gehrke SA, Júnior JA, Treichel TLE, do Prado TD, Dedavid BA, de Aza PN. Effects of insertion torque values on the marginal bone loss of dental implants installed in sheep mandibles. Sci Rep. 2022 Jan 11;12(1):538. doi: 10.1038/s41598-021-04313-5. PMID: 35017552; PMCID: PMC8752839.
27. Roca-Millan E, González-Navarro B, Domínguez-Mínger J, Marí-Roig A, Jané-Salas E, López-López J. Implant insertion torque and marginal bone loss: A systematic review and meta-analysis. Int J Oral Implantol (Berl). 2020;13(4):345-353. PMID: 33491366.
28. Amari Y, Piattelli A, Apaza Alccayhuaman KA, Mesa NF, Ferri M, Iezzi G, Botticelli D. Bone healing at non-submerged implants installed with different insertion torques: a split-mouth histomorphometric randomized controlled trial. Int J Implant Dent. 2019 Dec 5;5(1):39. doi: 10.1186/s40729-019-0194-2. PMID: 31802302; PMCID: PMC6893005.
29. De Santis D, Cucchi A, Rigoni G, Longhi C, Nocini PF. Relationship Between Primary Stability and Crestal Bone Loss of Implants Placed with High Insertion Torque: A 3-Year Prospective Study. Int J Oral Maxillofac Implants. 2016 Sep-Oct;31(5):1126-34. doi: 10.11607/jomi.4594. PMID: 27632269.
30. Stocchero M, Toia M, Cecchinato D, Becktor JP, Coelho PG, Jimbo R. Biomechanical, Biologic, and Clinical Outcomes of Undersized Implant Surgical Preparation: A Systematic Review. Int J Oral Maxillofac Implants. 2016 Nov/Dec;31(6):1247-1263. doi: 10.11607/jomi.5340. PMID: 27861649.
31. Duyck J, Corpas L, Vermeiren S, Ogawa T, Quirynen M, Vandamme K, Jacobs R, Naert I. Histological, histomorphometrical, and radiological evaluation of an experimental implant design with a high insertion torque. Clin Oral Implants Res. 2010 Aug;21(8):877-84. doi: 10.1111/j.1600-0501.2010.01895.x. Epub 2010 Apr 30. PMID: 20528892.
32. S. Weiner e H. D. Wagner, «THE MATERIAL BONE: Structure-Mechanical Function Relations,» Annual Review of Material Science, vol. 28, pp. 271-98, 1998.
33. C. H. Jacobs; M. H. Pope; J. T. Berry; F. Hoaglund, Journal o Biomechanics, vol. 7, pp. 131-136, 1974.
34. H. Peterlik, P. Roshger, K. Klaushofer e P. Fratzl, «Orientation dependent fracture toughness of lamellar bone,» International Journal of Fracture, vol. 139, pp. 395-405, 2006.
35. H. Peterlik, P. Roshger, K. Klaushofer e P. Fratzl, «From brittle to ductile fracture of bone,» Nature Material, vol. 5, pp. 52-55, 2006.
36. M. E. Merchant, «Mechanics of the metal cutting process. 1. Orthogonal Cutting and a Type 2 chip,» Journal of Applied Physics, vol. 16, pp. 267-275, 1945.
37. T. Nomura, E. Gold, M. P. Powers, S. Shingaki e J. L. Katz, «Micromechanics - structure relationship in the human mandible,» Dental Materials, vol. 19, pp. 167-173, 2003.
38. Y. Zhang, J. A. Robles-Linares, L. Chen, Z. Liao e A. J. Shih, «Advanced in machining of hard tissue - From material removal mechanism to tooling solution,» International Journal of Machinine Tools and Manufacture, vol. 172, 2022.
39. Z. Liao e D. A. Axinte, «On chip formation mechanism in orthogonal cutting of bone,» International Journal of Machine Tools and Manufacture, vol. 102, pp. 41-55, 2016.
40. J. A. Robles-Linares, Z. Liao, D. Axinte e A. Gameros, «The effect of interstitial fluid on the machining behaviour of cortical bone,» Journal of Material Processing Tech, vol. 307, 2022.
41. S. Kalpakjian e S. R. Schmitdt, Tecnologia meccanica, Milano: Pearson Italia, 2014.
42. J. Lee, B. A. Gozen e O. B. Ozdoganlar, «Modeling and experimentation of bone drilling force,» Journal of Biomechanics, vol. 45, pp. 1076-1083, 2012.
43. M. Basiaga e J. Szewczenko, «Numerical and experimental analyses of drills used in osteosynthesis,» Acta of Bioengineering and Biomechanics, vol. 13, n. 4, pp. 29-36, 2011.
44. Bosshardt DD, Salvi GE, Huynh-Ba G, Ivanovski S, Donos N, Lang NP. The role of bone debris in early healing adjacent to hydrophilic and hydrophobic implant surfaces in man. Clin Oral Implants Res. 2011 Apr;22(4):357-64. doi: 10.1111/j.1600-0501.2010.02107.x. PMID: 21561477.
45. Lang NP, Salvi GE, Huynh-Ba G, Ivanovski S, Donos N, Bosshardt DD. Early osseointegration to hydrophilic and hydrophobic implant surfaces in humans. Clin Oral Implants Res. 2011 Apr;22(4):349-56. doi: 10.1111/j.1600-0501.2011.02172.x. PMID: 21561476.
46. Rossi F, Lang NP, De Santis E, Morelli F, Favero G, Botticelli D. Bone-healing pattern at the surface of titanium implants: an experimental study in the dog. Clin Oral Implants Res. 2014 Jan;25(1):124-31. doi: 10.1111/clr.12097. Epub 2013 Jan 4. PMID: 23289845.
47. S. Karmani e F. Lam, The design and function of surgical drills and K-wires, Biomechanics, vol. 18, pp. 484-490, 2004.
48. S. Saha, S. Pal e J. Albright, Surgical Drilling: Design and performance of an improved drill, Journal of Biomechanical Engineering, vol. 104, p. 245, 1982.

49. Canullo L, Iacono R, Pires Godoy E, Punzo A, Cavicchia A, Gianfreda F, Bollero P. Hybrid Funnel Technique: A Novel Approach for Implant Site Preparation: A Pilot Study. Dent J (Basel). 2022 Aug 25;10(9):157. doi: 10.3390/dj10090157. PMID: 36135152; PMCID: PMC9497956.
50. Ikar M, Grobecker-Karl T, Karl M, Steiner C. Mechanical stress during implant surgery and its effects on marginal bone: a literature review. Quintessence Int. 2020;51(2):142-150. doi: 10.3290/j.qi.a43664. PMID: 31781692.
51. Khayat PG, Arnal HM, Tourbah BI, Sennerby L. Clinical outcome of dental implants placed with high insertion torques (up to 176 Ncm). Clin Implant Dent Relat Res. 2013 Apr;15(2):227-33. doi: 10.1111/j.1708-8208.2011.00351.x. Epub 2011 May 20. PMID: 21599832.
52. Kitamura E, Stegaroiu R, Nomura S, Miyakawa O. Biomechanical aspects of marginal bone resorption around osseointegrated implants: considerations based on a three-dimensional finite element analysis. Clin Oral Implants Res. 2004 Aug;15(4):401-12. doi: 10.1111/j.1600-0501.2004.01022.x. PMID: 15248874.
53. Kanayama M, Ferri M, Guzon FMM, Asano A, Alccayhuaman KAA, Rossi EF, Botticelli D. Influence on marginal bone levels at implants equipped with blades aiming to control the lateral pressure on the cortical bone. An experimental study in dogs. Oral Maxillofac Surg. 2024 Sep;28(3):1139-1149. doi: 10.1007/s10006-024-01228-z. Epub 2024 Mar 2. PMID: 38429433.
54. Ferreira Balan V, Ferri M, Pires Godoy E, Artioli LG, Botticelli D, Silva ER, Xavier SP. Controlled Lateral Pressure on Cortical Bone Using Blade-Equipped Implants: An Experimental Study in Rabbits. Bioengineering (Basel). 2024 Aug 16;11(8):835. doi: 10.3390/bioengineering11080835. PMID: 39199793; PMCID: PMC11352121.